Angewandte Chemie
Eine Zeitschrift der Gesellschaft Deutscher Chemiker

Supporting Information

Origin of Thermal and Hyperthermal CO_2 from CO Oxidation on Pt Surfaces: The Role of Post-Transition-State Dynamics, Active Sites, and Chemisorbed CO_2

Linsen Zhou, Alexander Kandratsenka, Charles T. Campbell, Alec M. Wodtke, and Hua Guo**

anie_201900565_sm_miscellaneous_information.pdf
anie_201900565_sm_Movie_pt111.wmv
anie_201900565_sm_Movie_Pt332.wmv

Supporting Information

S-I. COMPUTATIONAL DETAILS

All periodic density functional theory (DFT) calculations were performed with the Vienna Ab Initio Simulation Package (VASP).[1] The electron exchange-correlation effects were treated within the generalized gradient approximation (GGA), using the Perdew–Wang (PW91) functional.[2] The flat surface of Pt(111) was modeled by a four-layer slab, which has a 3×3 unit cell with the top three layers relaxed. The stepped surface of Pt(332) has large (111) terraces with steps spaced by six atomic rows. Here, we used a 1×4 surface unit cell (1.327 nm perpendicular to step edge x 4 Pt-Pt distances parallel to step edge) with four atomic layers, three of which were relaxed. Note that these two models, as used with one adsorbate structure per unit cell, correspond to different coverages, but with both coverages so low that this difference is not expected to impact the adsorption energies significantly. Adsorbates on the same site are slightly less stable on the (332) model. Since this is in the opposite direction of known coverage effects (CO and O are less stable at higher density), this must be due either to the proximity of the step edge or intrinsic errors in the DFT models The valence electrons were expanded with plane waves with a cutoff energy of 400 eV, while the projector augmented wave (PAW) method was used for the core electrons.[3] The Brillouin zone integration was performed using the *k*-point grids of 4 × 4 × 1 and 3 × 2 × 1 for the flat and stepped surfaces, respectively. A Fermi-Dirac smearing with a width of 0.1 eV was employed to help convergence.

The geometries were optimized using a conjugate-gradient method and the saddle points were determined using the climbing image nudged elastic band (CI-NEB) method[4] with a force convergence criterium of 0.02 eV·Å $^{-1}$. Bader charge analysis[5] was performed to identify atomic charges. The adsorption energy is defined as $E_{\mathrm{ads}} = E_{\mathrm{total}} - E_{\mathrm{slab}} - E_{\mathrm{adsorbate}}$, where E_{total}, E_{slab}, and $E_{\mathrm{adsorbate}}$ are energies of the total system, the bare surface, and the isolated gas-phase atom/molecule, respectively.

The calculated bulk lattice constant of Pt was found to be 3.982 Å, which agrees with the experiment value of 3.916 Å.[6] The optimized bulk lattice parameter was multiplied by a factor of 1.0049 (4.002 Å) for simulating the lattice at the experimental temperature of 593 K, using the known expansion (0.49%) from 0 to 593 K.[6]

Using the same DFT protocol, the AIMD simulations started from the optimized TS1

geometry. The atoms were assigned with random initial velocities, which are scaled to make the average kinetic energy equal to the average kinetic energy of a Boltzmann distribution at 593 K, the experimental temperature.[7] 100 trajectories for each Pt surface were propagated with a micro-canonical NVE ensemble - that is, an ensemble with constant number, volume, and energy - using the leap-frog algorithm implemented in VASP. The time step was set to 1.0 fs and the trajectories were propagated until the CO_2 center-of-mass reaches 6.0 Å above the surface with the velocity pointing away from the surface. The total energy was conserved within 40 meV for all trajectories. For the CO_2 product, vibrational quantum numbers for various modes were determined by normal-mode analysis (NMA)[8] as described in our previous work.[9] A three-dimensional potential energy surface for the free CO_2 used in the NMA calculations was pre-calculated using the same DFT method and fit with the permutation invariant polynomial-neural network approach.[10]

S-II. ADDITIONAL RESULTS

S-IIa. CO* + O* → CO_2* on Pt(111)

For CO adsorption on Pt(111), the calculated adsorption energy is −1.62 and −1.78 eV on the atop and hollow sites, respectively. These values compare reasonably well with the recent experimental adsorption energy of −1.47 ± 0.04 eV.[11] Similar to previous DFT calculations,[12] the standard DFT calculations fail to predict the experimentally observed atop-site preference and they overestimate the CO adsorption energy. This is known as the "CO/Pt(111) puzzle".[13] Even though some more advanced methods, such as the random phase approximation,[14] are capable of giving the adsorption energy close to the experimental value and predicting the correct atop adsorption site, they are still too expensive for AIMD calculations. Hence, we focus on the post-transition state dynamics for the formation of CO_2, which avoids the CO adsorption problem. The calculated absorption configurations of CO on Pt(111) and adsorption energies are shown in **Figure 1** and **Table S1**.

For O atom adsorption, the favorable adsorption sites are the hollow sites with the binding energy of –4.50 and –4.09 eV at the *fcc* and *hcp* sites, which are in agreement with previous theoretical results with the PW91[15] and PBE functionals,[16] and with the experimental value of –4.32 eV.[17] The absorption configurations of O on Pt(111) and adsorption energies are shown in **Figure 1** and **Table S1**

For the adsorption of CO_2, there are two types of adsorption states on transition-metal surfaces.[18] On Pt(111), the physisorbed CO_2 molecule is linear and lays parallel to the surfaces with the molecular center-of-mass ~3.4 Å from the nearest metal atom; this interaction is weak (−0.03 eV) and nearly independent of the lateral position of the adsorbate. The length of both C−O bonds is ∼1.18 Å, and the bond angle of OCO is 179.7°, close to the geometry of the gas-phase CO_2 molecule. The second adsorption state is a chemisorbed CO_2 that possesses a bent structure with a bond angle of 132.8° where one strongly interacting C−O bond (C−O1) is ∼2.1 Å above the surface and the other "free" C−O bond (C−O2) points away from the surface. The length of C−O1 and C−O2 bonds are 1.29 and 1.21 Å, respectively, both larger than the gas-phase bond length of linear CO_2. The bent geometry is formed by partial electron transfer from the Pt surface to CO_2, which carries a negative charge of −0.35 *e*. On the Pt(111) facet, the chemisorbed CO_2 has a positive adsorption energy of 0.37 eV with respect to gas-phase CO_2, but it is metastable because of a barrier between the chemisorbed and physisorbed wells. Our results on the physisorbed states of CO_2 are in generally good agreement with the previous DFT calculations, [19] other than the fact that no previous theory reported the chemisorbed CO_2 on Pt surfaces. The adsorption configurations of chemisorbed CO_2 on Pt(111) are shown in **Figure S1** and the geometric parameters and charge are given in **Table S2**.

To test the influence of van der Waals (vdW) corrections, we have calculated the adsorption energies with both the D2 and D3 correction schemes.[20] Since there are no PW91 parameters available for D3, parameters of the closely related PBE functional were used.[21] The calculated D3 corrected adsorption energy of the physisorbed or chemisorbed CO_2 is −0.30 or −0.05 eV relative to gaseous CO_2, which is lowered by 0.27 or 0.42 eV from the PW91 results of −0.03 or 0.37 eV, respectively. Both of these values are similar to previous work using the D2 correction (−0.22 and −0.03 eV).[22] However, the inclusion of dispersion always lead to a significant overestimate of the adsorption energy of CO.[23] The values are −1.94 eV for the D3 correction and −2.09 eV for the D2 correction,[22] which are much larger than the experimental one (−1.47 ± 0.04 eV).[11] As a result, no dispersion correction was used in our AIMD calculations.

The energetics and geometries along the Path TR1 for the terrace reaction of CO oxidation on the terrace site of the Pt(111) surface is shown in **Figure S2**, along with the geometries of the key species in **Table S3**. The first step is the combination of the adsorbed CO at a atop site and O at the second nearest *fcc* site to form the chemisorbed CO_2. At the transition state (TS1), the O atom

moves toward the adsorbed CO and forms a C-O bond with 1.96 Å length above a *hcp* site with an OCO angle of 110°, while spectator CO moiety sits on an atop site with its bond slightly lengthened from 1.16 to 1.17 Å, implying an "early" barrier resembling the reactant species. This step proceeds with the barrier of 1.00 eV, which agrees with previous DFT results of 1.05 eV[24] and 1.16 eV,[25] and the experimental barrier of about 1.0 eV.[26] These values are larger than some (~0.8 eV) obtained using calculations with another (PBE) functional.[19a, 27] The second step in the reaction is the transformation of the bent chemisorbed CO_2 to the linear physisorbed one, which has never been reported before. From **Figure S2**, the activation energy for this step is 0.21 eV, and transition state (TS2) has two equal CO bonds of 1.20 Å and a bond angle of 150.1°. After TS2, the physisorbed CO_2 product should desorb directly because of the shallow well (–0.03 eV).

S-IIb. CO* + O* → CO_2* on Pt(332)

The Pt(332) surface has (111) terraces of six-atom width separated by monoatomic (110) steps. In general, low-coordinated Pt surface atoms at the step edges strongly interact with adsorbates,[28] and the step sites are often more reactive than those on terraces.[29] In our calculations, CO was found to adsorb preferentially at the atop site of the upper step edge, and has a CO bond length of 1.16 Å and a C-Pt bond length of 1.87 Å, and is tilted toward the (110) orientation. The adsorption energy on the upper step edge is –1.97 and –1.86 eV for atop and bridge sites, respectively, which are quite similar to those of atop and bridge sites of the Pt(110) surface located on the (111) microfacets,[30] but more favorable by –0.35 and –0.10 eV than those on the Pt(111) surface. Hollow sites close to the step edge have the adsorption energies of about –1.70 eV, similar to those on the Pt(111) surface. The absorption configurations of CO on Pt(332) and adsorption energies are shown in **Figure 1** and **Table S1**.

The O atom is preferentially adsorbed at the bridge and *fcc* sites of the upper step edge with adsorption energies of –4.48 and –4.55 eV, which are consistent with a previous DFT study.[31] The adsorption energy at the *hcp* site near the upper step edge is 0.40 eV weaker than that of the corresponding *fcc* site on Pt(332). The O atom has a strong adsorption energy of –4.36 eV at the atop site of the lower step, comparing with the weaker adsorption of –3.66 eV on the atop site of upper step. The stable adsorption of the O atom at the bridge site of the upper step edge and atop site of the lower step edge is known to cause at moderate oxygen pressures the formation of one-dimensional PtO_2 stripes along the step, which has been found to play an important role in

carbon monoxide oxidation.[32] This scenario is not considered in this work because the O coverage is generally quite low in the experiments to which we are comparing our work. The absorption configurations of O on Pt(332) and adsorption energies are shown in **Figure 1** and **Table S1**.

Physisorbed CO_2 has a small adsorption energy of −0.09 eV near the step edge, which is similar to that on the Pt(111) surface. Not surprisingly, the physisorbed CO_2 has a structure almost identical to the gas-phase CO_2. For the chemisorbed state, CO_2 can absorb at different bridge sites near the step edge with the different binding energies ranging from −0.20 to +0.47 eV. The only stable one is at the bridge site of the upper step edge with adsorption energy of −0.20 eV. It is interesting that the adsorption energy becomes positive as C or O in the strongly interacting C−O1 bond is moved away from upper step edge, although all of the chemisorbed states have a similar structure with the C−O1 bond of ~1.29 Å, C−O2 bond of ~1.22 Å, and OCO angle of ~130°. The bent geometry of the chemisorbed CO_2 is due to the transfer of fractional electron charge from Pt to the antibonding orbital of CO_2, which prefers a bent geometry. There is a strong correlation between the amount of negative charge on chemisorbed CO_2 and the bending angle, as shown in **Table S2**. The absorption configurations of chemisorbed CO_2 on Pt(332) are shown in **Figure S1** and the geometric parameters and charges are given in **Table S2**.

Again, the inclusion of the dispersion forces using D2 or D3 corrections typically increases the adsorption energy. For instance, the adsorption of physisorbed or chemisorbed forms of CO_2 in the SR1 Path is lowered by 0.21 or 0.25 eV to −0.30 or −0.45 eV, respectively, using the D3 correction.

In **Figures S3 – S6**, the energetics of the reaction Paths SR1 – SR4 for step reactions are shown with the corresponding stationary point geometries. The geometric parameters of the transition states are given in **Table S3**. We focus on Path SR1 of CO oxidation, which has the lowest reaction barrier and a stable chemisorption well. Starting from the precursor states of co-adsorbed CO and O on an atop site of the step edge with a distance of 3.16 Å, the reactants moves toward each other and reach the TS1 saddle point. TS1 is again an "early" barrier, which has the C−O1 bond length of 2.01 Å on a bridge site of the step edge, the C−O2 bond of 1.17 Å toward the vacuum, and the OCO angle of 115.8°. The intrinsic reaction coordinate from TS1 leads to a stable bent CO_2 at the step edge. The chemisorption state can then overcome an activation barrier of 0.29 eV to the physisorption state. In TS2, both CO bonds are at 1.20 Å and

the OCO angle enlarges to 159.5°. The physisorption state resembles the gas-phase CO_2 with a very shallow (−0.09 eV) well.

S-IIc. Comparison of DFT activation energies to the experiment

In the recent experiment,[7] three reactions were identified with different activation energies relative to three different initial states: (1) both CO and O bound at terrace sites ($E_{a,1}$ = 0.6±0.1 eV), (2) CO at a terrace with O at step site ($E_{a,2}$ = 0.4±0.1 eV), and (3) both CO and O at step sites ($E_{a,3}$ = 0.65±0.1 eV). These were determined by analyzing rate-versus-coverage data using extremely low coverage CO gas pulses with a model that assumed rate constants (and thus activation energies) that are independent of coverage. Thus, we interpret these three experimental activation energies here to correspond to the energy increase between isolated adsorbates in the sites defined above and their appropriate transition states to make CO_2 (which requires steps that move the reactants together). These energies agree reasonably well with the transition state TS1 energies shown in **Figure 2**, if we assume that reaction (1) defined above goes through TS1 in TR1 on Pt(111) and that both reactions (2) and (3) go through the lowest-energy transition state near steps, i.e., TS1 in SR1 on Pt(332). The calculated energy difference between TS1 in TR1 on Pt(111) and isolated CO on its most stable (111) terrace site (F0 in **Figure 1**) plus isolated O on its most stable (111) terrace site (F0 in **Figure 1**) is 1.16 eV. The calculated energy difference between TS1 in SR1 on Pt(332) and isolated CO on its most stable (332) terrace site (F4 in **Figure 1**) plus isolated O on its most stable (332) step site (F2 in **Figure 1**) is 0.90 eV. The calculated energy difference between TS1 in SR1 on Pt(332) and isolated CO on its most stable (332) step site (A2 in **Figure 1**) plus isolated O on its most stable (332) step site (F2 in **Figure 1**) is 1.09 eV. While the absolute barrier heights of these reactions are uniformly 0.5 eV higher than the experimentally derived activation energies, there relative energies are similar to experiment. The systematic overestimate of the absolute value of the TS1 energies by DFT may be partially due to the neglect of dispersion forces here. This overestimate helps explain why CO_2 product from the step-step reaction's transition state (TS1 in SR1) is found by AIMD to have somewhat more excess energy than seen in the experiments. Due to neglect of dispersion, the depth of the CO_2 chemisorption well may also be underestimated in our model. This would explain why the calculated CO_2 translational energies in both channels are larger than in experiments. If this well is deeper, we would expect a longer trapping lifetime for chemisorbed CO_2, allowing more energy dissipation.

S-IId. AIMD results

A. Lifetime distributions

The distributions of the lifetimes of chemisorbed CO_2 on the Pt surfaces are shown in **Figure S7**. The lifetime is defined as the time required for trajectories initiated at the TS1 geometry to reach a 4 Å distance from the surface. Two lifetime distributions are shown for trajectories initiated at TS1 of the terrace (TR1) (red) and step reactions (SR1) (black), respectively. The lifetime distributions are quite different for these two reaction pathways. On the Pt(111) terrace site the most probable lifetimes are near ~200 fs, whereas for the 332 step reaction the distribution has a peak at 900 fs with a long tail extending to more than 2 ps. The long lifetime for the step site reaction is obviously due to trapping in the chemisorption well. The trajectories show that on the terrace site, decent from TS1 is sufficiently rapid that chemisorbed CO_2 cannot be trapped; whereas on steps, trapping is likely.

B. Product energy disposal and dissipation

The vibrational state distribution of the CO_2 is determined from the trajectories using the NMA method. The NMA method determines the vibrational energy within a separable harmonic oscillator approximation (details given in SI). As shown **Figure S8**, all three vibrational modes of the product are excited.

The average energy releases into different CO_2 product degrees of freedom are listed in **Table S4**. The energy loss to the surface, $\langle E_{loss} \rangle$, is defined as the total available energy - the saddle point energy of TS1 and the initial kinetic energy ($3k_BT/2$) of the three atoms (0.23 eV) - less the internal and translational energy of the CO_2 product. The total available energy is 1.70 eV for the terrace reaction and 1.16 eV for step reaction. On the terrace site, most of the available energy is disposed into the translational and vibrational modes. Only a small portion is dessipated into substrate. This low energy loss to the surface is presumably due to the frequency and mass mis-match between C, O and Pt degrees of freedom as well as the short time spent near the surface. The energy loss distributions are shown in **Figure S9**. At the step site, however, the vibrational modes represents the single largest portion of the disposed energy. Interestingly, the CO_2 product has a positve energy loss of 2.3%, indicating that most of the CO_2 products gain thermal energy from the surface. Recall that a surface temperature of 593 K is used in the dynamical model.

Both surface sites have the same average vibrationalenergy of about 0.80 eV and all three

vibrational modes are highly excited, as discused in the main text. This is presumably due to the similar geometries of TS1, which imparts the energy mostly into the vibrational modes, as suggested by the SVP results. At the terrace site, the desorption is fast and direct. Even at the step site, the residence time in the chemisorption well is not sufficiently long to dissipate the vibrational energy into Pt atom motion. But adiabatic vibrational energy loss to the solid has been assumed – should electronically nonadiabatic dissipation pathways be important, this result could be an artefact of the theory's assumptions. More future work is needed to explore this issue.

References:

[1] a) G. Kresse, J. Furthmuller, *Phys. Rev. B* **1996**, *54*, 11169-11186; b) G. Kresse, J. Furthmuller, *Comp. Mater. Sci.* **1996**, *6*, 15-50.

[2] J. P. Perdew, Y. Wang, *Phys. Rev. B* **1992**, *45*, 13244–13249.

[3] P. E. Blöchl, *Phys. Rev. B* **1994**, *50*, 17953-17979.

[4] G. Henkelman, B. P. Uberuaga, H. Jónsson, *J. Chem. Phys.* **2000**, *113*, 9901-9904.

[5] a) R. F. W. Bader, *Acc. Chem. Res.* **1985**, *18*, 9-15; b) G. Henkelman, A. Arnaldsson, H. Jónsson, *Comput. Mat. Sci.* **2006**, *36*, 354-360.

[6] a) J. W. Arblaster, *Platinum Met. Rev.* **1997**, *41*, 12-21; b) J. W. Arblaster, *Platinum Met. Rev.* **2006**, *50*, 118-119.

[7] J. Neugebohren, D. Borodin, H. W. Hahn, J. Altschäffel, A. Kandratsenka, D. J. Auerbach, C. T. Campbell, D. Schwarzer, D. J. Harding, A. M. Wodtke, T. N. Kitsopoulos, *Nature* **2018**, *558*, 280-283.

[8] a) G. Czakó, J. M. Bowman, *J. Chem. Phys.* **2009**, *131*, 244302; b) J. C. Corchado, J. Espinosa-Garcia, *Phys. Chem. Chem. Phys.* **2009**, *11*, 10157-10164.

[9] L. Zhou, B. Jiang, M. Alducin, H. Guo, *J. Chem. Phys.* **2018**, *149*, 031101.

[10] B. Jiang, H. Guo, *J. Chem. Phys.* **2014**, *141*, 034109.

[11] K. Golibrzuch, P. R. Shirhatti, J. Geweke, J. Werdecker, A. Kandratsenka, D. J. Auerbach, A. M. Wodtke, C. Bartels, *J. Am. Chem. Soc.* **2015**, *137*, 1465-1475.

[12] a) G. Marek, E. Andreas, H. Jürgen, *J. Phys. Condens. Mat.* **2004**, *16*, 1141; b) F. Abild-Pedersen, M. P. Andersson, *Surf. Sci.* **2007**, *601*, 1747--1753; c) M. Alaei, H. Akbarzadeh, H. Gholizadeh, S. de Gironcoli, *Phys. Rev. B* **2008**, *77*, 085414; d) A. Stroppa, G. Kresse, *New J. Phys.* **2008**, *10*, 063020.

[13] P. J. Feibelman, B. Hammer, J. K. Nørskov, F. Wagner, M. Scheffler, R. Stumpf, R. Watwe, J. Dumesic, *J. Phys. Chem. B* **2001**, *105*, 4018-4025.

[14] L. Schimka, J. Harl, A. Stroppa, A. Grüneis, M. Marsman, F. Mittendorfer, G. Kresse, *Nat. Mat.* **2010**, *9*, 741.

[15] T. Ogawa, A. Kuwabara, C. A. J. Fisher, H. Moriwake, T. Miwa, *J. Phys. Chem. C* **2013**, *117*, 9772-9778.

[16] Z. Gu, P. B. Balbuena, *J. Phys. Chem. C* **2007**, *111*, 9877-9883.

[17] Y. Y. Yeo, L. Vattuone, D. A. King, *J. Chem. Phys.* **1997**, *106*, 392-401.

[18] H. J. Freund, M. W. Roberts, *Surf. Sci. Rep.* **1996**, *25*, 225-273.

[19] a) C. Dupont, Y. Jugnet, D. Loffreda, *J. Am. Chem. Soc.* **2006**, *128*, 9129-9136; b) S.-G. Wang, X.-Y. Liao, D.-B. Cao, C.-F. Huo, Y.-W. Li, J. Wang, H. Jiao, *J. Phys. Chem. C* **2007**, *111*, 16934-16940; c) X. Liu, L. Sun, W.-Q. Deng, *J. Phys. Chem. C* **2018**, *122*, 8306-8314.

[20] a) S. Grimme, *J. Comput. Chem.* **2006**, *27*, 1787-1799; b) S. Grimme, J. Antony, S. Ehrlich, H. Krieg, *J. Chem. Phys.* **2010**, *132*, 154104.

[21] S. Gohr, S. Grimme, T. Söhnel, B. Paulus, P. Schwerdtfeger, *J. Chem. Phys.* **2013**, *139*, 174501.

[22] J. Ko, B.-K. Kim, J. W. Han, *J. Phys. Chem. C* **2016**, *120*, 3438-3447.

[23] P. Janthon, F. Viñes, J. Sirijaraensre, J. Limtrakul, F. Illas, *J. Phys. Chem. C* **2017**, *121*, 3970-3977.

[24] A. Alavi, P. Hu, T. Deutsch, P. L. Silvestrelli, J. Hutter, *Phys. Rev. Lett.* **1998**, *80*, 3650-3653.
[25] L. Grabow, Y. Xu, M. Mavrikakis, *Phys. Chem. Chem. Phys.* **2006**, *8*, 3369-3374.
[26] G. Ertl, *Surf. Sci.* **1994**, *299-300*, 742-754.
[27] a) A. Eichler, *Surf. Sci.* **2002**, *498*, 314-320; b) X.-Q. Gong, Z.-P. Liu, R. Raval, P. Hu, *J. Am. Chem. Soc.* **2004**, *126*, 8-9.
[28] B. Hammer, O. H. Nielsen, J. K. Nrskov, *Catal. Lett.* **1997**, *46*, 31-35.
[29] a) J. T. Yates, *J. Vac. Sci. Technol. A* **1995**, *13*, 1359-1367; b) P. Gambardella, Ž. Šljivančanin, B. Hammer, M. Blanc, K. Kuhnke, K. Kern, *Phys. Rev. Lett.* **2001**, *87*, 056103.
[30] S. Yamagishi, T. Fujimoto, Y. Inada, H. Orita, *J. Phys. Chem. B* **2005**, *109*, 8899-8908.
[31] R. Jinnouchi, K. Kodama, Y. Morimoto, *J. Electroanal. Chem.* **2014**, *716*, 31-44.
[32] J. G. Wang, W. X. Li, M. Borg, J. Gustafson, A. Mikkelsen, T. M. Pedersen, E. Lundgren, J. Weissenrieder, J. Klikovits, M. Schmid, B. Hammer, J. N. Andersen, *Phys. Rev. Lett.* **2005**, *95*, 256102.

Table S1. Adsorption Energies (eV) of CO and O on Pt(111) and Pt(332) surface sites labeled in **Figure 1**.

	A0	A1	A2	A3	A4	B2	F0	F1	F2	F3	F4	H0	H1	H2	H3	H4
CO	-1.62	-1.57	-1.97	---	-1.53	-1.86	-1.78	-1.70	-1.75	-1.54	-1.78	-1.75	-1.67	-1.66	-1.22	-1.75
O	-3.14	-3.06	-3.66	-4.36	-3.09	-4.48	-4.50	-4.29	-4.55	-4.13	-4.40	-4.09	-4.01	-4.15	-3.56	-4.01

Table S2. Geometric parameters and adsorption energies E_{ads} for different chemisorbed CO_2 in **Figure S1**. d_{C-Pt}, d_{C-O1}, and d_{C-O2} are distances of the C−Pt, C−O1, and C−O2 bonds, respectively. θ_{OCO} and q are the OCO bond angle and net Bader charge of CO_2, respectively.

Structure	E_{ads} (eV)	d_{C-Pt} (Å)	d_{C-O1} (Å)	d_{C-O2} (Å)	θ_{OCO} (deg)	q (e)
G1	−0.20	2.07	1.29	1.22	133.3	−0.37
G2	0.12	2.09	1.29	1.21	131.7	−0.39
G3	0.31	2.09	1.29	1.21	131.5	−0.36
G4	0.19	2.07	1.28	1.22	134.3	−0.39
G5	0.46	2.11	1.29	1.21	132.6	−0.37
G6	0.16	2.09	1.29	1.22	128.4	−0.42
G7	0.47	2.13	1.22	1.28	132.6	−0.39
G8	0.31	2.08	1.29	1.21	131.5	−0.39
G9	0.35	2.08	1.29	1.21	131.8	−0.38
G10	0.29	2.09	1.29	1.21	132.2	−0.35
on Pt(111)	0.37	2.10	1.29	1.21	132.8	−0.35

Table S3. Geometric parameters for TS1 and TS2 in different reaction paths in **Figure 2**. d_{C-Pt}, d_{C-O1}, and d_{C-O2} are the distances of the C−Pt, C−O1, and C−O2 bonds, respectively. θ_{OCO} is the OCO bond angle.

Transition state	Reaction Path	d_{C-Pt} (Å)	d_{C-O1} (Å)	d_{C-O2} (Å)	θ_{OCO} (deg)
TS1	SR1	1.93	2.02	1.17	106.8
	SR2	1.93	1.98	1.17	109.8
	SR3	1.92	2.12	1.16	99.3
	SR4	1.93	1.96	1.17	110.6
	TR1	1.93	1.96	1.17	110.0
TS2	SR1	2.59	1.21	1.19	159.5
	SR2	2.42	1.22	1.20	149.3
	SR3	2.52	1.22	1.19	149.9
	SR4	2.52	1.22	1.18	152.6
	TR1	2.38	1.22	1.20	150.1

Table S4. Average translational, rotational, and vibrational energies (in eV) of desorbed CO_2. The values in the parentheses are the percentage of the total available energy.

Reaction Path	$<E_{tran}>$	$<E_{rot}>$	$<E_{vib}>$	$<E_{loss}>$
TR1	0.64±0.08 (39.2%±4.7%)	0.16±0.05 (9.8%±2.9%)	0.82±0.08 (50.3%±4.8%)	−0.07±0.03 (4.3%±2.0)
SR1	0.14±0.03 (12.8%±3.0%)	0.18±0.04 (16.5%±3.3%)	0.80±0.05 (73.4%±4.0%)	0.03±0.02 (2.8%±1.5%)

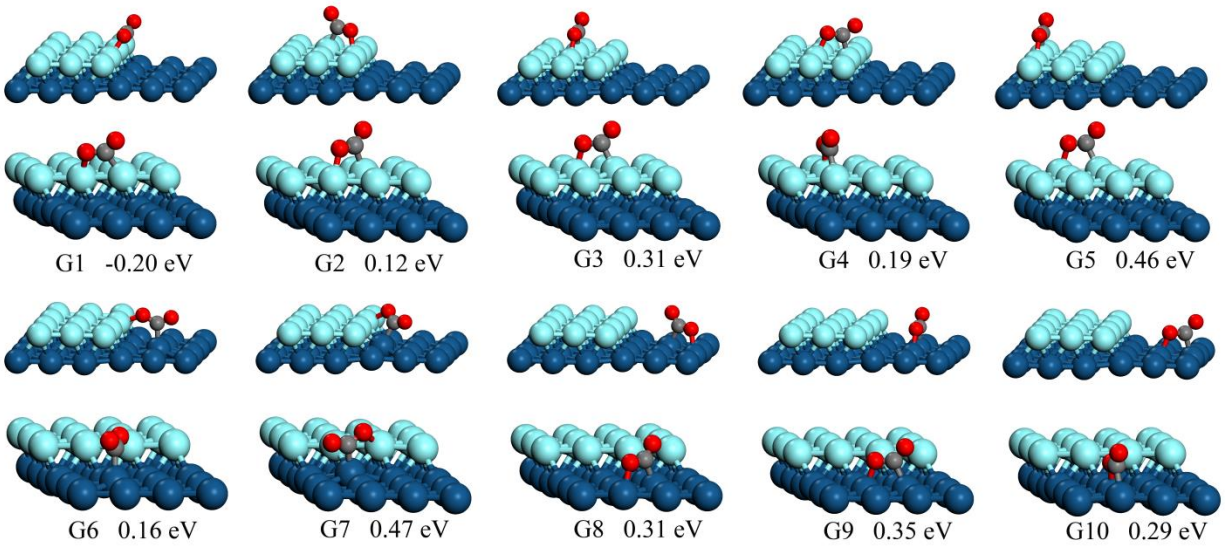

Figure S1. Optimized geometries of CO_2 chemisorbed on different Pt(332) sites. Also shown are the calculated CO_2 adsorption energies at these sites.

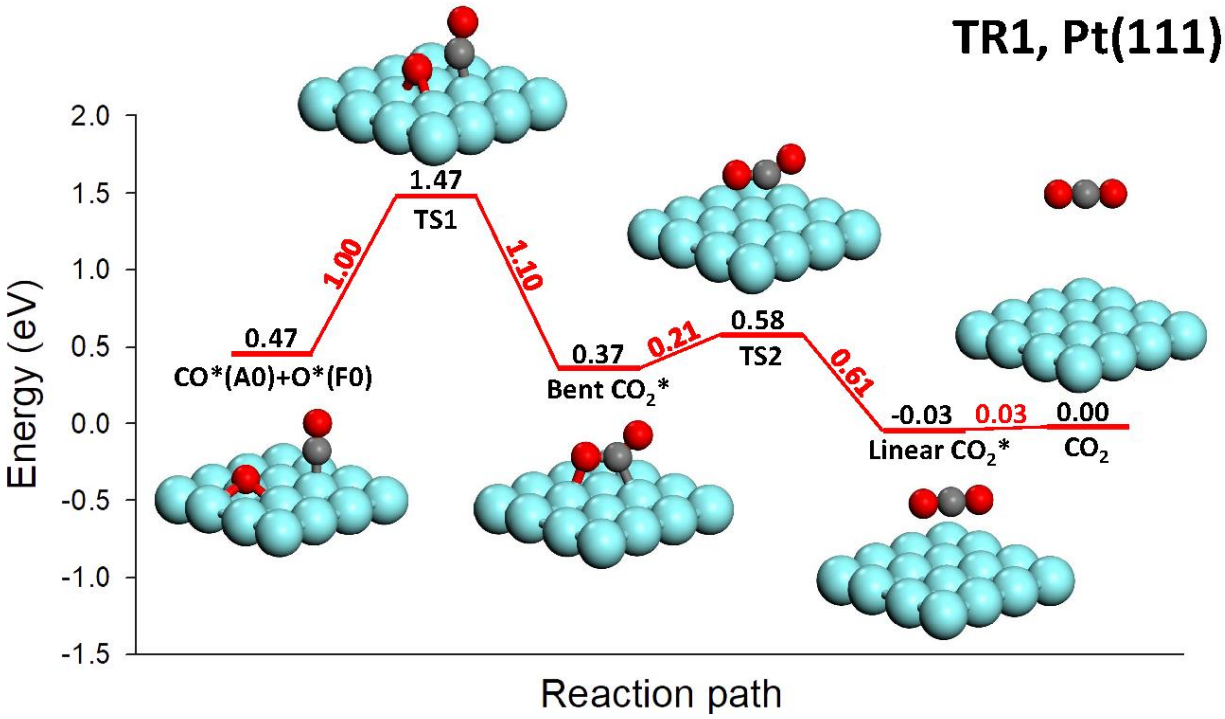

Figure S2. Energetics and geometries of the TR1 Path for CO oxidation on Pt(111). The CO* and O* are initially absorbed at neighboring A0 and F0 sites, respectively.

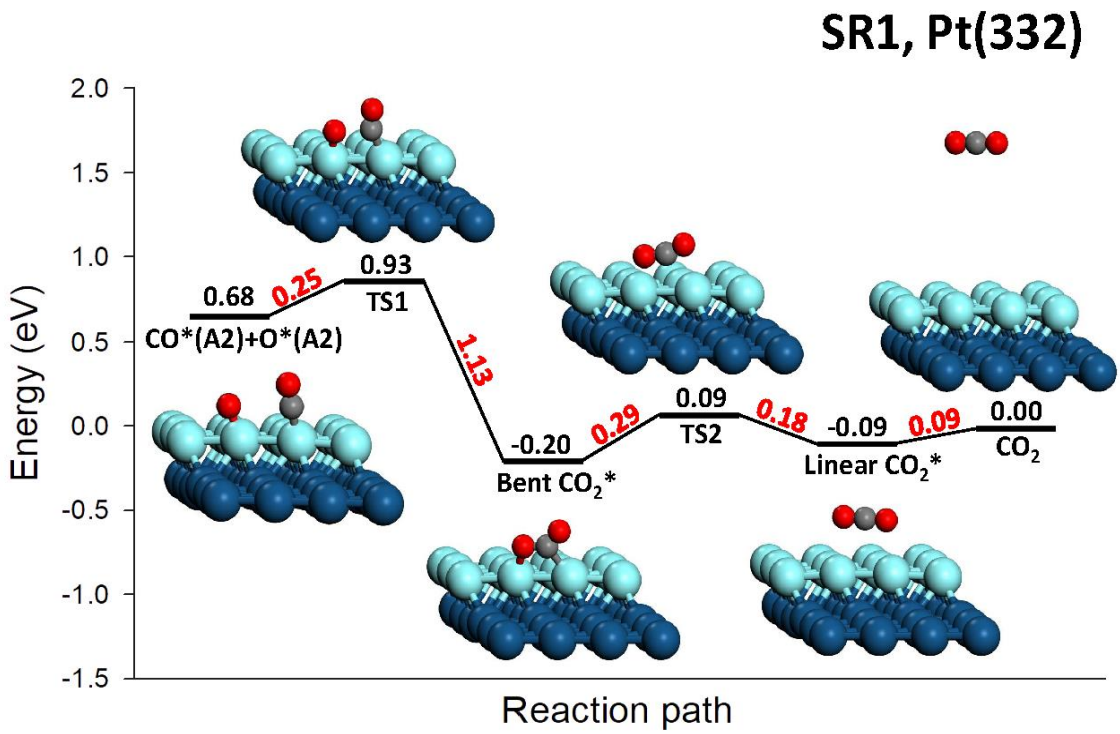

Figure S3. Energetics and geometries of the SR1 Path for CO oxidation on Pt(332). Both CO* and O* are initially absorbed at nearest-neighbor A2 sites, respectively.

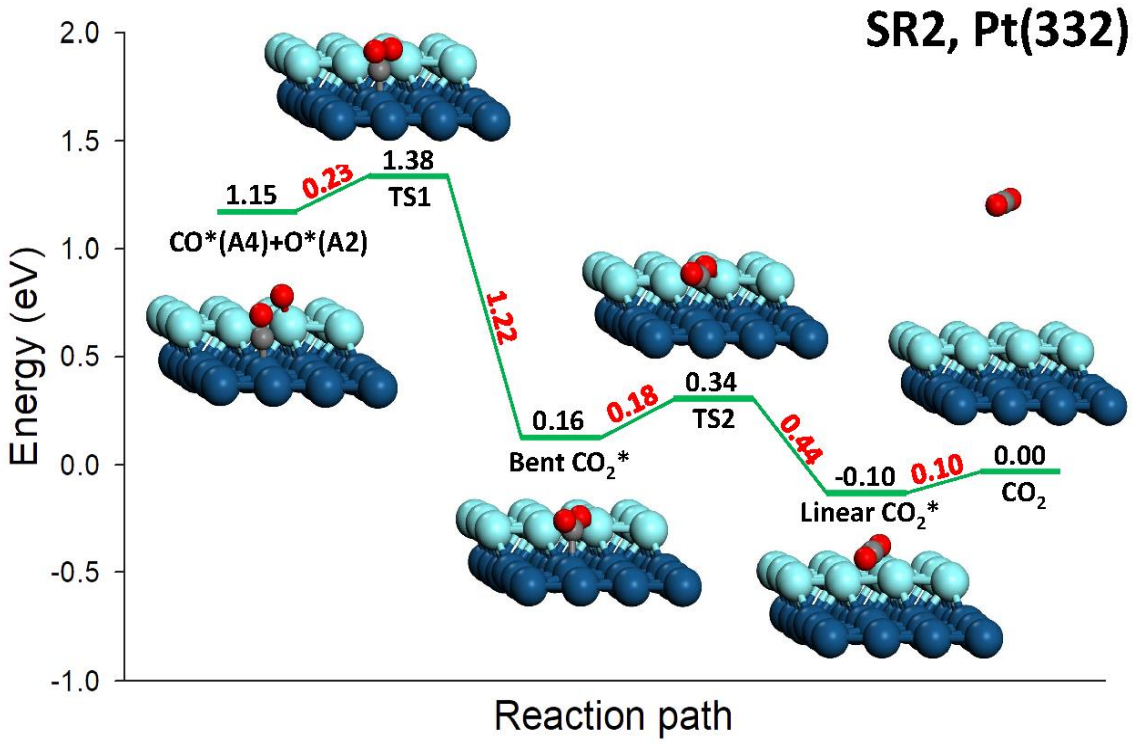

Figure S4. Energetics and geometries of the SR2 Path for CO oxidation on Pt(332). The CO* and O* are initially absorbed at nearby A4 and A2 sites, respectively.

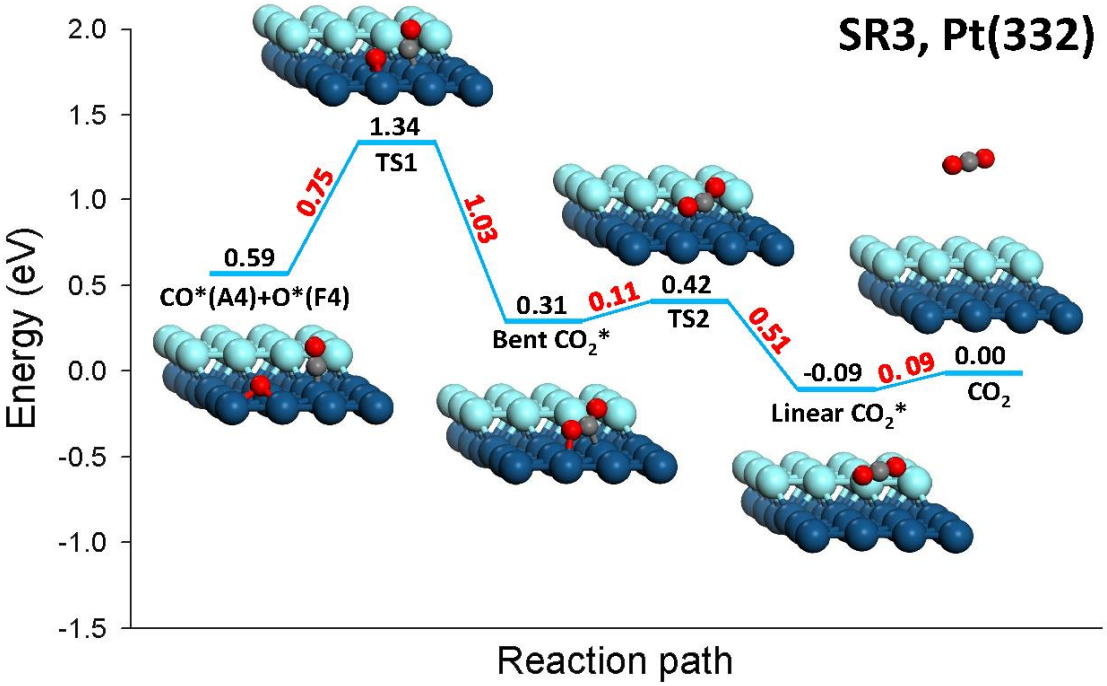

Figure S5. Energetics and geometries of the SR3 Path for CO oxidation on Pt(332). The CO* and O* are initially absorbed at nearby A4 and F4 sites, respectively.

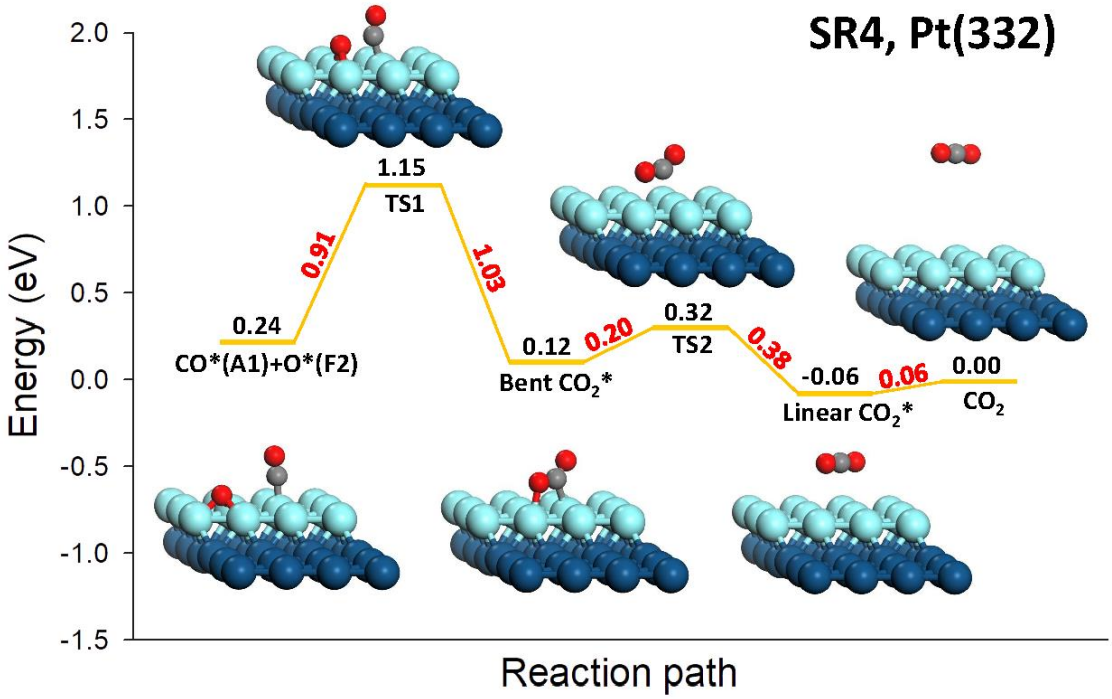

Figure S6. Energetics and geometries of the SR4 Path for CO oxidation on Pt(332). The CO* and O* are initially absorbed at nearby A1 and F2 sites, respectively.

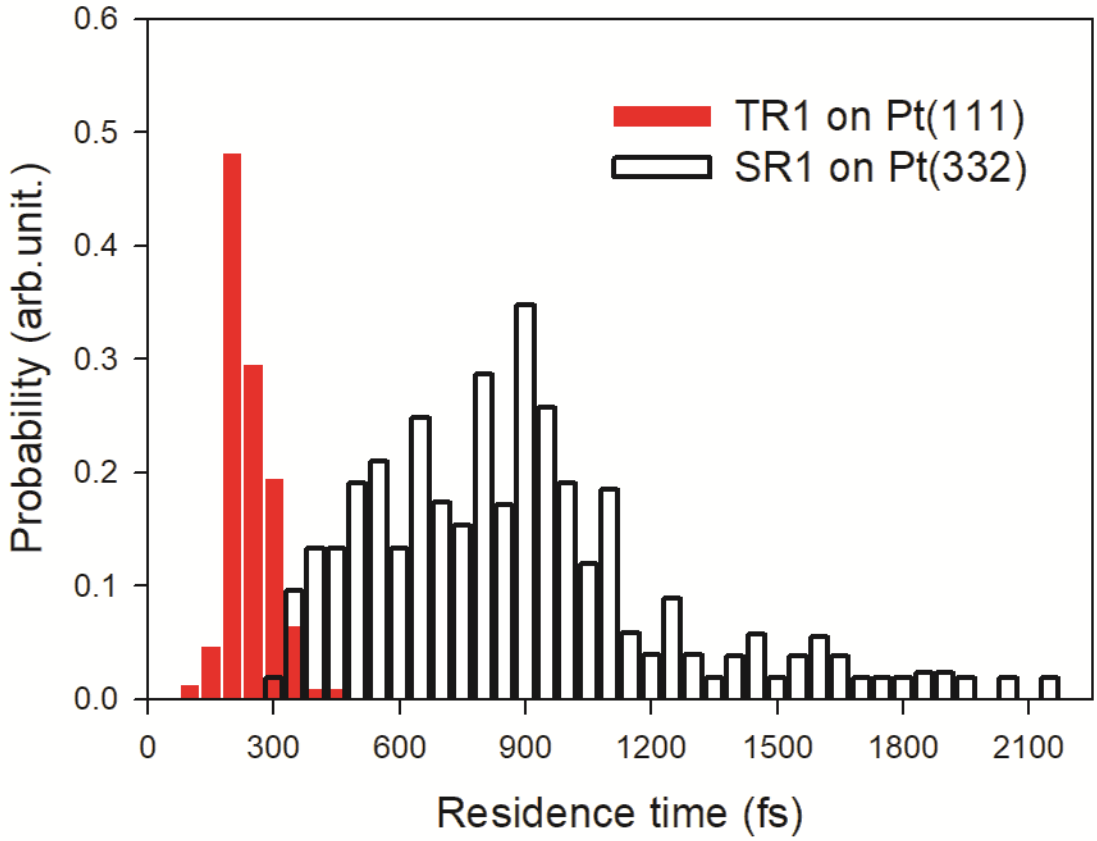

Figure S7. Calculated residence time distributions for CO_2 in the TR1 and SR1 Paths on Pt(111) and Pt(332), respectively.

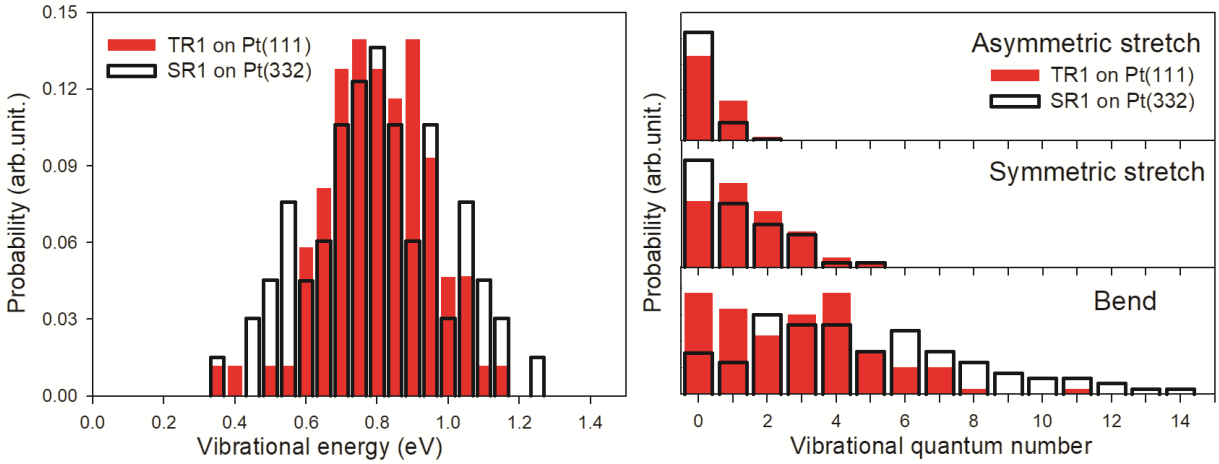

Figure S8. Calculated vibrational state distributions of desorbed CO_2 from the terrace and step sites on Pt(111) and Pt(332).

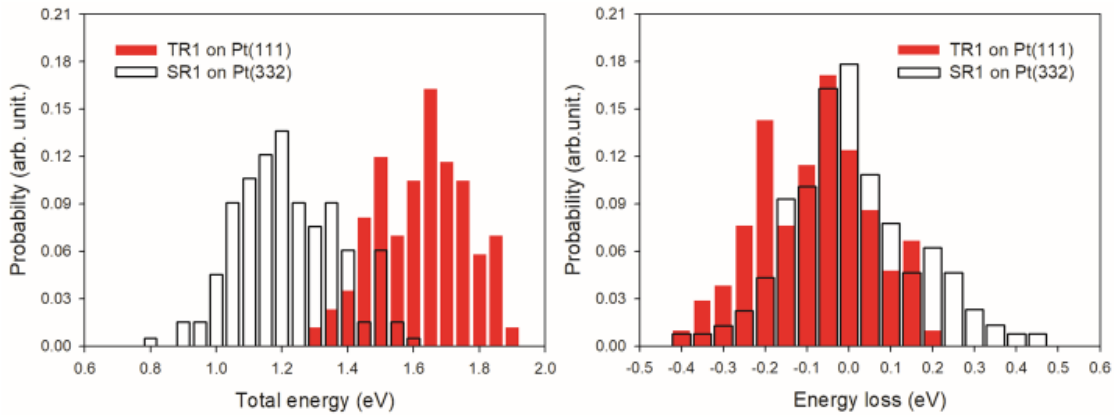

Figure S9. Total energy distributions and energy loss distributions of the CO_2 product in the TR1 and SR1 Paths on Pt(111) and Pt(332), respectively.